Tr. J. of Physics
23 (1999) , 77 – 87.

The Renormalization-Group Microscope: The Local Statistical Mechanics of Heterogeneous Systems

Dicle YEŞİLLETEN
Department of Physics, Massachusetts Institute of Technology
Cambridge, Massachusetts 02139, USA
A. Nihat BERKER
Department of Physics, Massachusetts Institute of Technology
Cambridge, Massachusetts 02139, USA
Department of Physics, İstanbul Technical University
80626 Maslak, Istanbul-TURKEY

Received ...

Abstract

Renormalization-group theory is developed to yield all local microscopic thermodynamic densities in heterogeneous systems. Local energy densities and local magnetizations are thus obtained for random-bond systems, random-field systems, and spin-glasses, in two and three dimensions. Different order-disorder mechanisms in these diverse systems, such as chaotic ordering and domain-wall melting, become quantitatively evident.

1. Introduction

From its inception, the renormalization-group method [1] was marked by a series of successes in statistical mechanics, from the calculation of critical exponents [1], to the determination of entire thermodynamic functions at or away from criticality [2], first-order phase transitions [3], and global phase diagrams [4]. The compounded difficulty presented by heterogeneous systems, namely systems with quenched (frozen-in) disorder, was also surmounted, yielding critical properties and phase diagrams [5–9]. Thermodynamic densities of heterogeneous systems were also obtained [6,8,9], but as averages across the entire system under study.

In fact, much more information of physical relevance is contained in the statistical mechanical formulation of heterogeneous systems and can be accessed [10] by renormalization-group theory, as demonstrated below. We present here a renormalization-group calculation of the local thermodynamic densities, namely local energy densities and local magnetizations, in heterogeneous systems. Since it yields the detailed equilibrium statistical

mechanics at the most microscopic scale, we call our method "the renormalization-group microscope". The method is widely applicable: In this paper, we present the microscopic thermodynamic densities for (1) random-bond systems, (2) random-field systems, and (3) spin-glass systems, obtaining the qualitatively different order-disorder mechanisms of each system [10].

2. The Renormalization-Group Method

2.1. General Approach

The renormalization-group method [1] is the iterative solution of a statistical mechanics problem. The latter is defined, for example, by local (spin) degrees of freedom $\{s_i\}$ arrayed on a lattice of sites labeled by i. These degrees of freedom are coupled by interactions of strengths J_{ij},H_i,..., as seen in the Hamiltonian

$$-\beta\mathcal{H}(\{s_i\}) = \sum_{<ij>} J_{ij}s_is_j + \sum_i H_is_i + \sum_i G_i + ... \tag{1}$$

The last shown term is an additive constant, whose value does not affect the physical properties of the system; however, this term is needed in the renormalization-group formalism, as it accumulates physical information of the finer scales, under the rescaling transformations of the method. In Eq.(1), $< ij >$ indicates summation over nearest-neighbor pairs of sites and, at each site i, the degree of freedom s_i can take the values of ± 1. All of the equilibrium properties of the system are contained within the partition function

$$Z = \sum_{\{s_i\}} e^{-\beta\mathcal{H}(\{s_i\})}, \tag{2}$$

where the sum is over all possible states of the local degrees of freedom, the spins $\{s_i\}$.

The renormalization-group method prescribes that the sum in Eq.(2) be carried out only over a subset of the local degrees of freedom, so chosen that their evaluation constitutes a scale change, without a structure change, in the system. The remaining summand can be cast as an exponentiated Hamiltonian, as in Eq.(1), but with changed (renormalized) values of the interaction strengths:

$$\sum_{\{s_i\}}^{\text{subset}} e^{-\beta\mathcal{H}(\{s_i\})} = e^{-\beta'\mathcal{H}'(\{s_i\}_{\text{remaining}})}, \tag{3}$$

where the prime indicates the presence of renormalized interactions. This transformation is recycled ad infinitum, and the entire statistical mechanics is thereby done.

2.2. Homogeneous Systems

In the case of homogeneous systems, the interactions are uniform across the system:

$J_{ij} = J$, etc. The renormalized interaction strengths are determined by the unrenormalized interaction strengths, via the so-called recursion relations,

$$\vec{K}' = \vec{R}\,(\vec{K}), \tag{4}$$

where $\vec{K} \equiv$ (J,H,G,...) and $\vec{R}\,(\vec{K})$ is a function deduced from the partial sum in Eq.(3). Repeated applications of Eq.(4) generate the renormalization-group flows in the space of $\vec{K}$. Under these flows, each distinct region of the phase diagram (i.e., each phase and each type of phase transition point) is attracted to its own fixed point. Thus, the global connectivity of the renormalization-group flows yields immediately the phase diagram in the variables in $\vec{K}$. Linear analysis at the fixed points of the second-order phase transitions yields the critical exponents.

The interaction strengths $\vec{K}$ are also referred to as the "thermodynamic fields". Conjugate to them are the "thermodynamic densities",

$$\vec{D} = \frac{1}{N}\frac{\partial}{\partial\,\vec{K}} \ln Z(\vec{K}) = (q < s_i s_j >, < s_i >, 1, ...), \tag{5}$$

where N is the number of lattice sites and q is the number of nearest-neighbor bonds per lattice site. A renormalization-group recursion relation for the densities is obtained with the chain rule,

$$\vec{D} = b^{-d}\,\vec{D}' \cdot \frac{\partial\,\vec{K}'}{\partial\,\vec{K}}, \tag{6}$$

where b is the length scale change factor and d is the spatial dimensionality. Repeated applications of Eq.(6) connect the densities between the initial point and the terminal point of a trajectory. Densities at the latter point are readily calculated, thus yielding the densities of any point in $\vec{K}$-space by initiation of a trajectory [11].

2.3. Heterogeneous Systems

When interaction strengths vary across the system, e.g., $J_{ij} \neq J_{kl}$ and/or $H_i \neq H_j$ in the Hamiltonian in Eq.(1), a heterogeneous system obtains. Ordering (of $\{s_i\}$) in the presence of frozen-in disorder (of $\{J_{ij}\}$ and/or $\{H_i\}$,...) is investigated [5]. The statistical mechanics problem acquires a compounded difficulty, but also the rewards of qualitatively new physical phenomena. Importantly different situations result from different types of frozen-in disorder, as seen below.

The phase diagram of a system with frozen-in (quenched) disorder is calculated, in renormalization-group theory, by the recursion, under scale change, of the distribution function $P(\{\vec{K}_{ij}\})$ of interaction strengths, as seen in several previous studies [6-9]. In the present work [10], we demonstrate that the most detailed microscopic description of local densities can be calculated by renormalization-group theory, revealing qualitatively different physical phenomena.

The local heterogeneous interactions $\vec{K}_{ij}$= (J_{ij},H_i,H_j,G_{ij},...) and the local heterogeneous densities $\vec{D}$= ($< s_i s_j >$,$< s_i >$,$< s_j >$,1,...) are related by the conjugate relation

$$\vec{D}_{ij} = \frac{\partial \ln Z}{\partial \vec{K}_{ij}}. \tag{7}$$

The recursion relation of the local densities is again obtained with the chain rule,

$$\vec{D}_{ij} = \sum_{<i'j'>} \vec{D}'_{i'j'} \cdot \frac{\partial \vec{K}'_{i'j'}}{\partial \vec{K}_{ij}}, \tag{8}$$

where $\vec{K}'_{i'j'}$ and $\vec{K}_{ij}$ are connected by a local recursion relation for interactions,

$$\vec{K}'_{i'j'} = \vec{R}\,(\{\vec{K}_{ij}\}), \tag{9}$$

deduced from the partial sum of the partition function. The interaction recursion relation being local in nature, in Eq.(9), for a given $i'j'$, $\vec{K}'_{i'j'}$ effectively depends on the unrenormalized interactions $\vec{K}_{ij}$ from a limited range in ij. Thus, in Eq.(8), for a given ij, a limited number of summand terms is non-negligible.

A system as large as desired can be reduced to a very small system, by repeated renormalization-group transformations. After each renormalization-group transformation, the content of Eq.(8) is accumulated by matrix multiplication, the product matrix relating the local densities of the original system and those of the repeatedly renormalized system. The consecutive applications of Eq.(9) track the renormalized local interactions. These interactions, at each renormalization-group step, determine the matrix in Eq.(8), which gets multiplied as just explained. Finally, the renormalized interactions of the very small system are used in the determination of its local densities, which, through the product matrix, determine all of the local microscopic densities of the original system. The inner workings of the renormalization-group microscope are hereby fully specified.

2.4. Calculation

As seen above, the renormalization-group microscope is perfectly general: it can use any local (therefore, position-space) renormalization-group transformation. In the present calculations, we have used the Migdal-Kadanoff procedure [12,13], due to its proven efficacy. We study Hamiltonians with the terms exhibited in Eq.(1), on square ($d = 2$) and cubic ($d = 3$) lattices. As a preliminary, given a spatial array of local interactions of different values, an exact rewriting of the Hamiltonian of Eq.(1) is

$$-\beta\mathcal{H}(\{s_i\}) = \sum_{<ij>} (J_{ij} s_i s_j + h_i s_i + h_j s_j + G_{ij}). \tag{10}$$

The renormalization-group transformation is illustrated in Fig.1. In the first (approximate) step of the transformation, all the bonds [terms in parentheses in Eq.(10)] in a

group of $b^d - b$ bonds are "moved" onto the b bonds in their midst. For heterogeneous systems, each moved interaction strength is added to the corresponding interaction strength of the closest unmoved neighbor or is equally shared for the case of several closest unmoved neighbors, this being done in one lattice direction at a time. In the second (exact) step of the transformation, the partition-function sums over the doubly coordinated sites are performed, resulting in renormalized interactions between the remaining sites. Thus, the local recursion relation of Eq.(9) takes the form, for *b=2*,

$$\begin{aligned} J'_{i'k'} &= \tfrac{1}{4}\ln[R(+,+)R(-,-)/R(+,-)R(-,+)], \\ h'_{i'} &= \tfrac{1}{4}\ln[R(+,+)R(+,-)/R(-,-)R(-,+)], \\ h'_{k'} &= \tfrac{1}{4}\ln[R(-,+)R(+,+)/R(+,-)R(-,-)], \\ G'_{i'k'} &= \tfrac{1}{4}\ln[R(+,+)R(+,-)R(-,-)R(-,+)] + \tilde{G}_{ij} + \tilde{G}_{jk}, \\ \text{with } R(s_i,s_k) &= \textstyle\sum_{s_j}^{\pm 1} \exp(\tilde{J}_{ij}s_is_j + \tilde{h}_is_i + \tilde{h}_js_j + \tilde{J}_{jk}s_js_k + \tilde{h}_js_j + \tilde{h}_ks_k), \end{aligned} \tag{11}$$

where $\tilde{J}_{ij}$, etc., are the bond-moved interaction strengths. For example, in $d = 2$ and for $b = 2$,

$$\begin{aligned} \tilde{J}_{ij} &= J_{ij} + (J_{kl} + J_{mn})/2, \\ \tilde{h}_i &= h_i + (h_k + h_m)/2, \\ \tilde{h}_j &= h_j + (h_l + h_n)/2, \\ \tilde{G}_{ij} &= G_{ij} + (G_{kl} + G_{mn})/2, \end{aligned} \tag{12}$$

where $< kl >$ and $< mn >$ are the nearest-neighbor parallels on each side of $< ij >$. In $d = 3$ and for $b = 2$,

$$\tilde{J}_{ij} = J_{ij} + \frac{1}{2}\sum_{<kl>_1} J_{kl} + \frac{1}{4}\sum_{<pr>_2} J_{pr}, \tag{13}$$

and similarly for the other interactions, where the first sum is over the four nearest-neighbor parallels to $< ij >$ and the second sum is over the four next-nearest-neighbor parallels to $< ij >$.

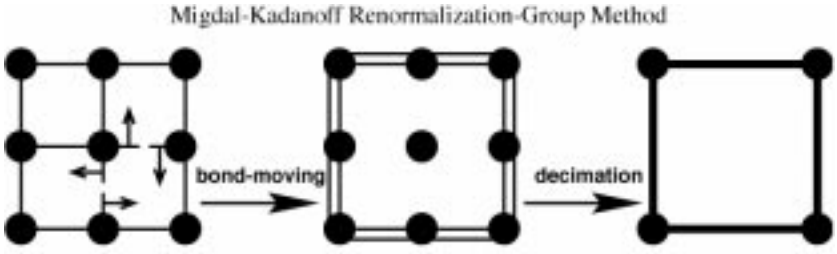

Figure 1. The Migdal-Kadanof procedure is extended to heterogeneous systems and used in the implementation of the renormalization-group microscope. Note that any other position-space renormalization-group transformation could be used in this implementation.

3. Results: Local Energy Densities

3.1. Quenched Random-Bond System

The quenched random-bond system is obtained from the general Hamiltonian of Eq.(1) by studying a system with

$$H_i = 0 \quad \text{and} \quad J_{ij} = \hat{J}_{ij}/T \tag{14}$$

with the coupling strengths chosen across the system according to the quenched Gaussian distribution

$$P(\hat{J}_{ij}) = (2\pi\sigma^2)^{-1/2} \exp[(\hat{J}_{ij} - \hat{J})^2/2\sigma^2]. \tag{15}$$

The results for all local energy densities $< s_i s_j >$, where i and j are nearest neighbors, are shown in Fig.2(a), at various temperatures T, for $d = 2$. It is seen that this heterogeneous system gains local energy rather uniformly across the system. The calculation also shows that local energy gain (equivalently, nearest-neighbor decorrelation) occurs, as temperature is raised, more readily along the edges of the system, as expected since these regions have weaker connectivity.

3.2. Spin-Glass System

The coupling-strength distribution used in the preceding section, Eq.(15), essentially excludes antiferromagnetic bonds, for the study of quenched randomness without the effects of frustration [14]. By contrast, here Eqs.(14) are used with the symmetric distribution

$$P(\hat{J}_{ij}) = [\delta(\hat{J}_{ij} + \hat{J}) + \delta(\hat{J}_{ij} - \hat{J})]/2. \tag{16}$$

This randomly assigns, across the system, ferromagnetic ($+\hat{J} > 0$) and antiferromagnetic ($-\hat{J}$) interactions with equal probability and a spin-glass system [15] is obtained. The results for all local energy densities $| < s_i s_j > |$ are shown in Fig.3(a), at various temperatures T, for $d = 2$. The contrast to the quenched random-bond system with no frustration (Sec.3.1) is striking. Firstly, the spin-glass gains local energy much more readily as temperature is increased. Even more striking is the non-uniformity of the local energy distribution in the spin-glass system. The calculation shows that local centers of frustration remain energetic to the lowest temperatures; as temperature is increased, locally energetic regions emanate from the centers of frustration; these regions connect, in turn leaving isolated localities of low energy at intermediate temperatures.

4. Results: Local Magnetizations

4.1. Quenched Random-Bond System

Calculation of local magnetizations $< s_i >$ (equivalently, local order parameters) yields insight into the contrasting order-disorder mechanisms in heterogeneous systems. The results for all local magnetizations of the quenched random-bond system [Eqs.

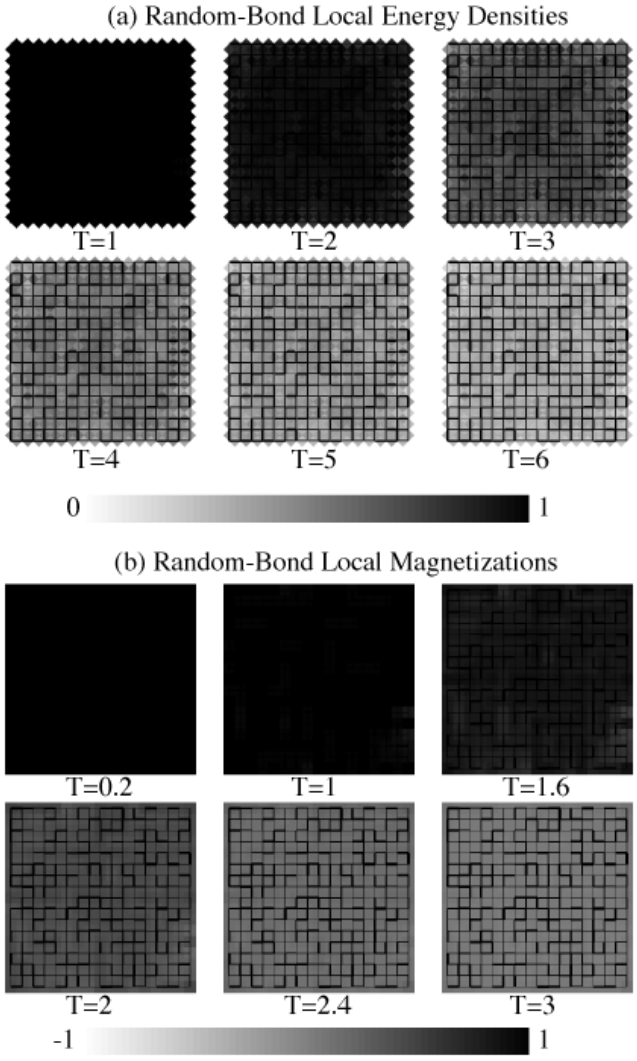

Figure 2. (a) The calculated array of local energy densities, i.e., nearest-neighbor correlations $< s_i s_j >$, for a random-bond system in $d = 2$, at increasing temperatures. This system is obtained from Eq.(1) by setting $H_i = 0$ and randomly choosing $\hat{J}_{ij}$ from a Gaussian distribution of mean $\hat{J} = 1$ and standard deviation $\sigma = 0.24$; these different bond strengths are represented in the figure by the thicknesses of the bonds. The values of $< s_i s_j >$ vary from 1 (black) for complete correlation, to 0.5 (grey) for intermediate correlation, to 0 (white) for no correlation. (b) The calculated array of local magnetizations $< s_i >$ for this random-bond system, at increasing temperatures. The values of $< s_i >$ vary from +1 (black) for up-alignment, to 0 (grey) for no-alignment, to –1 (white) for down-alignment. A nucleation field of $\hat{H}_i = 0.02$ has been applied to the boundary spins.

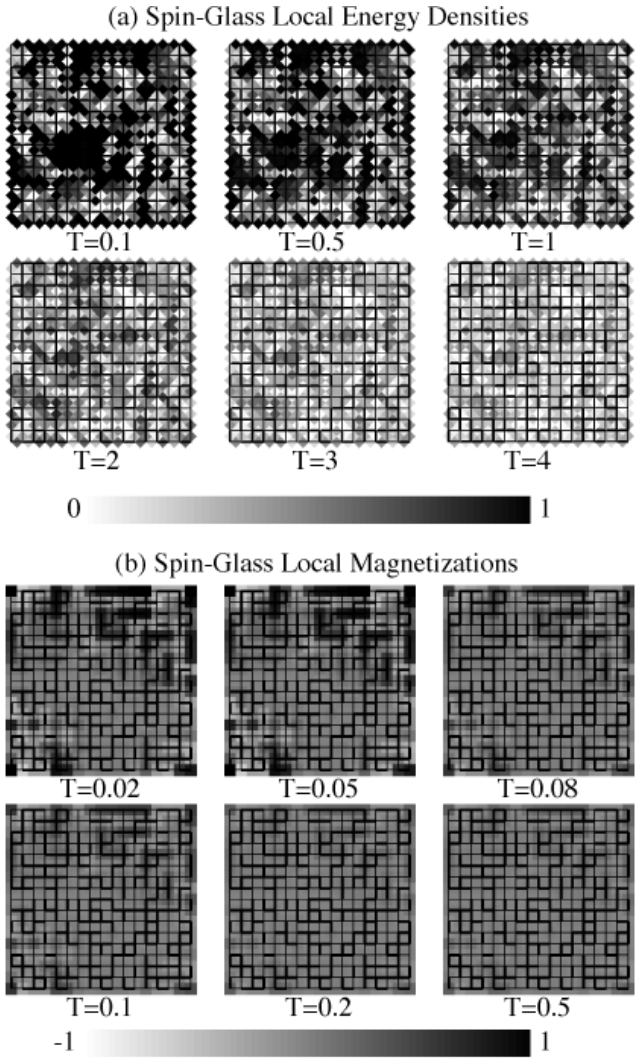

Figure 3. (a) The calculated array of local energy densities, i.e., nearest-neighbor correlations $| < s_i s_j > |$, for a spin-glass system in $d = 2$, at increasing temperatures. This system is obtained from Eq.(1) by setting $H_i = 0$ and randomly choosing $\hat{J}_{ij}$ as +1 or –1, respectively represented by thick or thin bonds in the figure. The values of $| < s_i s_j > |$ vary from 1 (black) for complete correlation, to 0.5 (grey) for intermediate correlation, to 0 (white) for no correlation. (b) The calculated array of local magnetizations $< s_i >$ for this spin-glass system, at increasing temperatures. The values of $< s_i >$ vary from +1 (black) for up-alignment, to 0 (grey) for no-alignment, to –1 (white) for down-alignment. A nucleation field of $\hat{H}_i = -0.004$ has been applied to the boundary spins.

(14),(15)] are shown in Fig. 2(b), at various temperatures T, for $d = 2$. Consistently with the picture from the local energy densities, rather uniform disorder across the system, with readier disordering along the edges, is observed.

4.2. Spin-Glass System

The contrast in spin-glass systems is again dramatic. The results for all local magnetizations of the spin-glass system [Eqs. (14),(16)] are shown in Fig.3(b), at various temperatures T, for $d = 2$. In two dimensions, the spin-glass system does not have true long-range order, but the low-temperature results here are an indication of the order that sets in as dimensionality is increased, between $d = 2$ and 3. Note that the order-parameter calculations are achieved with a small symmetry-breaking field along the edges of the system (see the figure captions), as dictated by rigorous statistical mechanics.

The results of Fig. 3(b) show that a *non-contiguous* subset of the spins order, i.e., become pinned in one or the other direction, as temperature is lowered. In-between these, spins are unpinned. This ordering picture had been deduced when renormalization-group transformations that became chaotic were first observed in frustrated systems [16].

4.3. Quenched Random-Field System

The quenched random-field system is obtained from the general Hamiltonian of Eq.(1) by studying a system with

$$J_{ij} = \hat{J}/T \tag{17}$$

with the field strengths H_i chosen across the system according to the distribution

$$P(H_i) = [\delta(H_i + H) + \delta(H_i - H)]/2. \tag{18}$$

The results for the local magnetizations were obtained for the entirety of a $d = 3$ system. They are exhibited for one plane within this $d = 3$ system in Fig.4(b), at various temperatures T. Yet another dramatically different order-disorder mechanism is observed. The spins, all aligned at low temperatures, disorder as temperature is increased by the formation of opposite, compact, contiguous domains. This is the Imry-Ma mechanism [17], valid at strong coupling. The calculation here reflects the fact that, under renormalization-group transformations, the intermediate temperatures where the phase transition occurs get mapped onto the neighborhood of a zero-temperature, i.e., strong-coupling fixed point. Fig.4(a) shows that anticorrelated spin neighbors occur in the regions intervening between the domains.

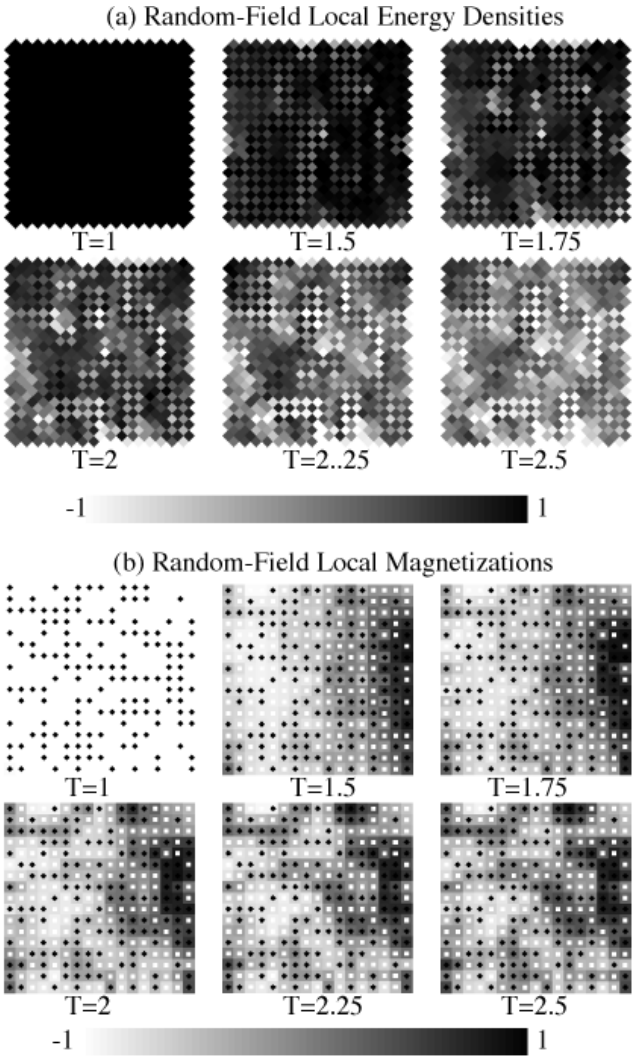

Figure 4. (a) The calculated array of local energy densities, i.e., nearest-neighbor correlations $< s_i s_j >$, for a random-field system in $d = 3$, at increasing temperatures. This system is obtained from Eq.(1) by setting $\hat{J}_{ij} = 1$ and randomly choosing H_i as +2.73 or –2.73. The values of $< s_i s_j >$ vary from +1 (black) for complete correlation, to 0 (grey) for no correlation, to –1 (white) for complete anticorrelation. (b) The calculated array of local magnetization for this random-field system, at increasing temperatures. The values of $< s_i >$ vary from +1 (black) for up-alignment, to 0 (grey) for no-alignment, to –1 (white) for down-alignment. In both (a) and (b), values for the same cross-section of the three-dimensional system is shown. In (b), the sites with H_i +2.73 or –2.73 are respectively shown by ♦ or □.

It is thus seen that detailed microscopic information on thermodynamic densities and physical mechanisms can be obtained from the renormalization-group microscope.

Acknowledgements

This research was supported by the MIT Center for Materials Science and Engineering Undergraduate Research Opportunities Program, by the US Department of Energy under Grant No. DE–FG02–92ER45473, and by the US National Science Foundation Grant No. DMR–94–00334.

References

[1] K.G. Wilson, *Phys. Rev. B*, **4** (1971) 3174, 3184.

[2] M. Nauenberg and B. Nienhuis, *Phys. Rev. Lett.*, **33** (1974) 944.

[3] B. Nienhuis and M. Nauenberg, *Phys. Rev. Lett.*, **35** (1975) 477.

[4] A.N. Berker and M. Wortis, *Phys. Rev. B*, **14** (1976) 4946.

[5] G. Grinstein and A. Luther, *Phys. Rev. B*, **13** (1976) 1359.

[6] S.R. McKay and A.N. Berker, *J. Appl. Phys.*, **64** (1988) 5785.

[7] M.S. Cao and J. Machta, *Phys. Rev. B*, **48** (1993) 3177.

[8] A. Falicov, A.N. Berker, and S.R. McKay, *Phys. Rev. B*, **51** (1995) 8266.

[9] A. Falicov and A.N. Berker, *Phys. Rev. Lett.*, **76** (1996) 4380.

[10] D. Yeşilleten and A.N. Berker, *Phys. Rev. Lett.*, **78** (1997) 1564.

[11] A.N. Berker, S. Ostlund, and F.A. Putnam, *Phys. Rev. B*, **17** (1978) 3650.

[12] A.A. Migdal, *Zh. Eksp. Teor. Fiz.*, **69** (1975) 1457 [*Sov. Phys. - JETP*, **42** (1976) 743].

[13] L.P. Kadanoff, *Ann. Phys. (N.Y.)*, **100** (1976) 359.

[14] G. Toulouse, *Commun. Phys.*, **2** (1977) 115.

[15] S.F. Edwards and P.W. Anderson, *J. Phys. F*, **5** (1975) 965.

[16] S.R. McKay, A.N. Berker, and S. Kirkpatrick, *Phys. Rev. Lett.*, **48** (1982) 767.

[17] Y. Imry and S.-k. Ma, *Phys. Rev. Lett.*, **35** (1975) 1399.